Picture-frame testing of woven prepreg fabric

An investigation of sample geometry and shear angle acquisition

Krogh, Christian; White, Kari D.; Sabato, Alessandro; Sherwood, James A.

Published in:
International Journal of Material Forming

DOI (link to publication from Publisher):
10.1007/s12289-019-01499-y

Publication date:
2020

Document Version
Accepted author manuscript, peer reviewed version

Picture-frame testing of woven prepreg fabric: An investigation of sample geometry and shear angle acquisition

Noname manuscript No.
(will be inserted by the editor)

Picture-Frame Testing of Woven Prepreg Fabric: An Investigation of Sample Geometry and Shear Angle Acquisition

Christian Krogh · Kari D. White · Alessandro Sabato · James A. Sherwood

Received: date / Accepted: date

Abstract This paper examines different concepts in relation to the picture-frame test for shear characterization of a woven prepreg fabric. The influence of the sample arms is investigated by means of cut slits as well as removed transverse tows. Shear angles are obtained using Digital Image Correlation (DIC) and also from images taken during the test which are processed for fiber angles directly from the weave texture. The image processing relies on the Hough transform in MATLAB. The concept of constant shear strain rate is discussed and implemented in the test software by a multi-linear crosshead velocity profile. Finally, bias-extension data are obtained and used for comparison. It is found that the sample arm modifications have a pronounced effect on the measured shear load whereas the uniformness of the shear strain field in the samples is not improved considerably.

Keywords Woven carbon fiber prepreg · Shear characterization · Picture frame testing · Image Analysis

1 Introduction

During the forming of woven fabrics, a significant amount of shear or trellising occurs. This deformation mechanism has long been recognized as the most important when an initially flat piece of fabric undergoes deformation to a double-curved shape (Nguyen et al., 1999). Naturally, the shear properties of the fabric must be characterized if the forming behavior is to be accurately predicted in a simulation code. To this end it is common practice to use either the *picture-frame test* or the *bias-extension test* to do this characterization.

The picture-frame test uses a square frame with hinged corners. A test sample is clamped in the frame with the fibers oriented parallel and perpendicular to the frame edges. One frame corner is held stationary while the opposite corner is displaced such that the sample theoretically is subjected to uniform shear. The test has been applied to a number of different materials such as thermoplastic woven glass fibers (Peng and Cao, 2005), dry woven carbon fibers (Nguyen et al., 1999), woven carbon fiber prepreg (Mohan et al., 2016), Uni-Directional (UD) carbon fiber prepreg (Harrison et al., 2002), and thermoplastic cross-ply polyethylene fiber sheets (Dangora et al., 2015).

There are a number of known issues in regard to the picture-frame test. First, the test is sensitive to the clamping boundary conditions as discussed by Harrison et al. (2004). If fiber tension across the sample is too low, the sample might not shear to the same extent as the frame. On the other hand, if the tension is too high, then the results might be compromised - especially if the sample is misaligned in the frame. Second, because of the frame design with the clamping area and the hinges, the samples are in general not square but cruciform. Therefore, the "arms" of the sample could also influence the measurements in the gage area in the center of the sample.

To avoid the contributions from the sample arms when testing woven materials, some researchers remove the transverse tows from the arms before testing, see e.g. Lussier (2000), Zhu et al. (2007), and Peng and Cao (2005). However, based on a benchmark study with

Christian Krogh (corresponding author)
Department of Materials and Production, Aalborg University, Denmark
E-mail: ck@mp.aau.dk

Kari D. White · Alessandro Sabato · James A. Sherwood
Department of Mechanical Engineering, University of Massachusetts Lowell, USA

contributions from several research groups (Cao et al., 2008) there exist no general practice regarding the sample arms. The results from the paper do in fact not suggest differences between samples with and without transverse tows in the sample arms. However, due to the many variations in test setups and practices among the participating research groups, this conclusion is not decisive. In the paper, it was discussed how one should be careful not to alter the sample tightness or local fiber orientations when removing the transverse tows.

For some materials, the transverse fibers are not so easily removed. Dangora et al. (2015) studied the effect of sample arms in the picture-frame test with thermoplastic preconsolidated UD cross-ply. Slits were cut in varying widths and also the polyurethane matrix was dissolved to achieve a condition of "infinite slits". A significant influence of the sample arms was found and only the infinite-slit condition test data provided good agreement in a finite element (FE) simulation.

In the picture-frame test, it is often assumed that the shear strains are uniform in the gage area such that a global shear force and shear strain can be obtained from a kinematic and static analysis of the frame. It is, however, common practice to use either Digital Image Correlation (DIC) measurements or to manually check the fiber angles from pictures of the test as a validation (Cao et al., 2008).

The manual identification of fiber angles from pictures can be alleviated by using image processing techniques. Harrison et al. (2008) presented a program that uses lines drawn on the samples before testing to identify the shear angles. However, the authors noted that the finite thickness and the varying contrast of the lines would introduce noise into the measurements. Arumugam et al. (2016) conducted picture-frame tests of 3D textiles with a grid drawn on the test samples. Pictures taken during the test were analyzed using a Hough transform to recognize straight lines. Other researchers have obtained fiber angles directly from the weave texture. See for instance the study by Olson et al. (2017) on parachute suspension lines. Lastly, it should be noted that advanced commercial laser measurement systems exist, which was e.g. applied by Krieger et al. (2015) for the bias-extension test of NCF.

A final point regarding the picture frame is, that it does not produce a constant shear angle rate when displaced at a constant crosshead rate. Rather, the shear angle rate is a nonlinear function of the crosshead movement. This statement is evident from the aforementioned kinematic relations between the crosshead displacement and the shear angle. The behavior must be taken into account when testing rate-dependent materials such as prepregs and e.g. comparing the test data to bias-extension data.

A number of remedies to the non-constant shear angle rate have been discussed in the literature. Harrison et al. (2002) used the picture-frame kinematics to generate a nonlinear crosshead vs. time expression that yields a constant shear rate. It was implemented on a standard universal test machine. However, additional control software was needed to achieve the nonlinear crosshead movement. It was reported that the use of a constant shear rate resulted in less variability in the data. In the study by Lebrun et al. (2003), picture-frame and bias-extension data were compared. The shear angle rate was taken into account by using a calculated ratio between the two crosshead speeds which ensured an equal (but varying) shear angle rate. Harrison et al. (2004) developed normalization equations for the picture-frame test and the bias-extension test that allows for comparison. By normalizing the two types of test data by their respective crosshead rates, good agreement was found in the comparison.

The overall goal of this paper is to investigate the shear characterization of a woven prepreg fabric using the picture-frame test. This investigation involves the influence of the cruciform sample arms on the gage area and how fabric shear angles can be acquired. Regarding the sample arms, the transverse tows are not easily removed due to the resin, and an approach similar to that of Dangora et al. (2015) will be taken, which involves cut slits and dissolved resin. The details hereof are presented in Section 2. The influence of the sample arms is inspected by considering the load required to shear the sample as well as the distribution of shear angles in the sample. Regarding the latter, the kinematic analysis does not suffice, for which reason a full-field method is needed. Here, the well-proven DIC is employed and it is also investigated if the fabric angles can be acquired based on the weave texture from images taken during the test. More specifically, the Hough transform is applied in this analysis. The data acquisition methods are presented in Section 3. The rate-dependency of the prepreg fabric is taken into account by testing at a constant shear rate. A nonlinear expression for the crosshead is generated and approximated using linear segments. The segments are readily implemented as ramps in the standard Instron® Bluehill software. The procedure is elaborated in Section 4. The results of the paper are presented in Section 5. It is shown that the sample arm modification mainly influences the measured shear load. To address potential issues with the clamping boundary conditions, the picture-frame data are compared to results from a bias-extension test. While this test has a number of drawbacks, the tows are

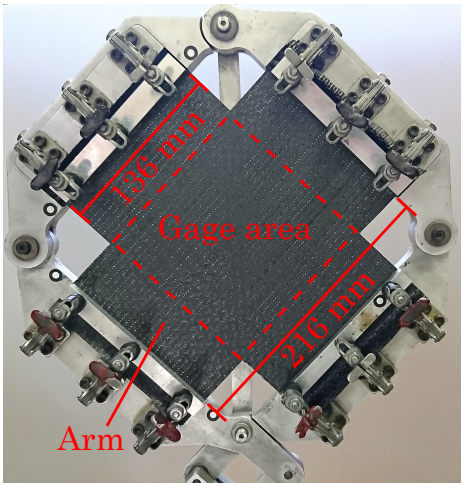

Fig. 1 The picture frame with a mounted sample. The frame has an amplifying linkage mechanism.

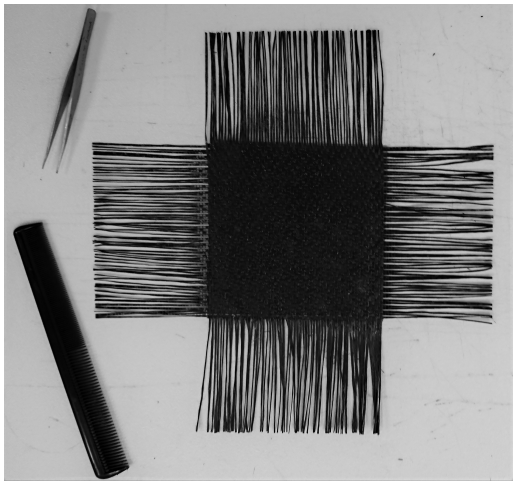

Fig. 2 Transverse tows removed from sample with comb and tweezers after submersion in ethanol.

always untensioned, and thus the test can be used to verify picture-frame data as suggested by Harrison et al. (2004). Good agreement between the two tests is found provided that the proper sample area-normalization is carried out. The paper is ended with a discussion in Section 6 and a conclusion.

2 Test Samples

The material used in this study is a 4-harness satin-weave carbon-fiber prepreg with a bismaleimide (BMI) resin. The thickness is 0.3 mm and the areal density is 314 g/m^2. The resin causes the material to exhibit viscoelasticity. As a consequence, the shear force required to shear the material depends on the rate of shear. This rate-dependency was verified in a previous study with the prepreg material using the bias-extension test (Krogh et al., 2019). The viscoelasticity makes the shear response different from that of dry fabrics. The testing temperature is also a factor because the viscosity of the resin is dependent on temperature. In this study, all tests were carried out at room temperature.

Figure 1 shows the picture frame including the amplifying linkage mechanism with a mounted sample. The amplifying linkage mechanism respectively increases the displacement and decreases the force on the frame by a factor of 4.25 in comparison to the crosshead values. The basic sample type is a cruciform with an arm width equal to 62 tows or approximately 136 mm, i.e. the maximum width that fits in the frame. The test sample is cut from the stock material by means of a utility knife and a ruler. The basic sample type serves as the reference and will be referred to as having *full arm geometry*. To investigate the influence of arm geometry, the basic sample is modified in two ways: By *cutting slits* and by *removing the transverse tows*.

The cutting of slits is likewise carried out with the utility knife and the ruler. The slits are cut with a distance increment of 3 tows, and thus, the total number of slits in each arm is 20.

To remove the transverse tows, the resin must be dissolved. For this purpose ethanol was selected because it dissolves the uncured BMI resin without damaging the carbon fibers according to chemical resistance charts. Each sample arm was submerged in a tray with ethanol for a few seconds after which excess ethanol was wiped off. Care was exercised not to get any ethanol on the gage area of the sample. Next, the sample was placed on a cutting board, and a ruler was placed on top on the boundary between the gage area and the arm. A comb was used to remove the transverse tows. Only a few tows were removed at a time, starting from the free edge. Near the gage area, tweezers were used to remove the final transverse tows. The end result is depicted in Fig. 2.

Using the approach outlined above, it was found, that the remaining tows would still be coated with resin. For the sake of easier mounting in the frame, it was decided not to remove that resin and thereby keep the fibers bundled. Also, in relation to the mounting of the sample in the frame, it was found preferable to comb the samples while on the cutting board and wrap the arm ends in masking tape before transferring the sample to the frame.

Both the cutting of slits and removing of transverse tows are cumbersome tasks that take about 10 - 15 minutes per sample. This time must be added to the cutting of the basic cruciform sample. If DIC is used,

(see Section 3.2) then even more time must be added for sample preparation.

A wooden fixture was made to keep the frame stable while mounting the sample. The fixture has a surface to support the sample which is flush with the frame. In this way, the effect of varying fiber tensions was diminished.

3 Data Acquisition and Processing

In this section, the different methods of data acquisition that were employed in the study are presented and discussed, i.e. data from the crosshead, DIC and image processing using Hough transform.

3.1 Crosshead Force and Displacement

Crosshead force and displacement were recorded in the picture-frame tests with the Instron Bluehill Universal Testing software. The load cell used had a capacity of 5 kN and an accuracy of 0.1 %. The formulas used to calculate the shear strain and shear force are typical for picture-frame analyses (Harrison et al., 2004; Cao et al., 2008; Launay et al., 2008; Jauffrès et al., 2010). The global shear angle, γ, of the sample is geometrically related to the length of the frame, L_F, and the crosshead displacement, δ through the equation:

$$\gamma = \frac{\pi}{2} - 2\arccos\left(\frac{1}{\sqrt{2}} + \frac{\delta}{2L_F}\right) \tag{1}$$

The shear force, F_{sh}, on the fabric is also a function of the global shear angle and the crosshead force, F:

$$F_{sh} = \frac{F}{2\cos\left(\frac{\pi}{4} - \frac{\gamma}{2}\right)} \tag{2}$$

Peng et al. (2004) used a method of normalization for cruciform sample testing based on energy conservation through work done per volume. Using an assumption of zero contribution of load from the arms and uniform shear deformation in the gage area, the shear force can be normalized over the gage area with side length L_f, while also taking the frame length into account. Combining these into a single expression yields (Jauffrès et al., 2010):

$$F_{sh,norm\_gage} = \frac{L_F}{L_f^2}\frac{F}{2\cos\left(\frac{\pi}{4} - \frac{\gamma}{2}\right)} \tag{3}$$

3.2 Digital Image Correlation

For digital image correlation, a sequence of digital images is compared to an initial reference image. A displacement field can be calculated from the local deformation of the isotropic pattern within a subset window or facet. Differentiation of the displacement field will yield the local strain of the sample. A strain window is used by the differentiation algorithm, defining the number of neighboring facets. A large strain field will yield less noise, but also less spacial resolution. Two cameras, installed at different angles with respect to the sample, are required for 3D DIC. Strains are calculated in the tangential plane of the object (Lomov et al., 2008).

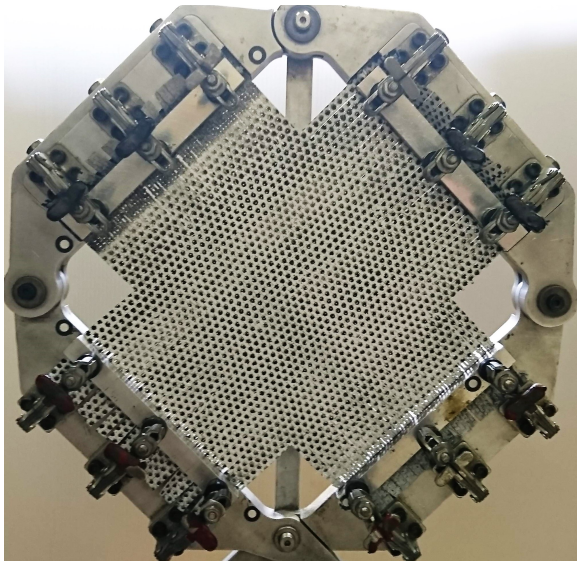

Fig. 3 Slitted arm sample with DIC pattern mounted in the frame.

Digital image correlation was performed with an Aramis 3D digital imaging setup. The specifications of the setup are found in Table 1. The analysis was performed with a facet size of 10 × 10, an 8-pixel step and linear shape function. The strain window was set to 3 points with the strain resolution being 0.05°. The samples were patterned by first applying a thin coat of white spray paint to reduce glare. A uniform dot pattern was then applied using lightly sprayed black paint with a stencil. The holes of the stencil were approximately 3 mm in diameter, spaced 5 mm center-to-center on the diagonal. The use of the stencil helped to achieve an even ratio of white and black paint as well as the right speckle size. Notice, that the size and spacing of the holes in the stencil are not a direct measure of the spatial resolution because the pattern is still considered random. The patterning of the sample mounted in the frame is shown in Fig. 3.

The previous discussion of DIC has illustrated, that the method relies on an applied pattern which enables the correlation between the deformed and the undeformed samples. The first question is whether the paint affects the measurements. This point is up for debate as some authors have reported that the paint applied for DIC does affect the results (Harrison et al., 2018) while

Table 1 DIC setup in Aramis. The shear strain resolution is computed as the standard deviation of two still image strain maps.

Technique used	3D DIC
Sensor and Digitization	1624 × 1236, 8 bit
Lens and Imaging Distance	8.5 mm, 0.6 m
Recording frequency	10 Hz
Facet, step	10 × 10, 8
Shape functions	Linear
Interpolation of 3D points	Max. 3 points
Filtering	Median 5 × 5, 3 runs
Strain window	3 points
Shear strain resolution	0.05°

others have reported that there is no influence (Jauffrès et al., 2010). In a comparison between different samples, it can be assumed that the paint affects all the samples equally (Dangora et al., 2015). Next, because the reference configuration is recorded after the sample has been mounted in the frame, it does not contain information about any possible unintended pre-deformation. That is, the fiber directions could be different from ±45° before the test is started. Lastly, the selection and application of a proper pattern can be a time consuming task. These issues are the motivation for looking into alternatives.

3.3 Image Processing using Hough Transform

The idea of the image processing setup is to identify the fiber angles directly from the weave texture which alleviates the issues discussed above. The tows will appear as straight lines in the images which can be detected using the Hough transform algorithm. The method is useful for finding lines in images, even if the input image contains sparse or broken lines (Marques, 2011). Figure 4 depicts the principle of the algorithm in Cartesian coordinates. The figure shows two coordinate systems, namely the *Cartesian space* and the *Transform domain*. In the Cartesian space, two points, (x_1, y_1) and (x_2, y_2), are located, which represent two points in a recorded image. The Transform domain represent possible lines in the image, i.e. on the form $y = ax + b$. Many lines passing through the point (x_1, y_1) can be generated and vice versa for the the point (x_2, y_2). Each of those lines map to a point in the transform domain. However, only one line passes through both points and that line is exactly given by the intersection point in the transform domain.

In practice, the algorithm operates in polar coordinates with the parameters ρ (perpendicular distance from the line to the origin) and θ (the angle between the

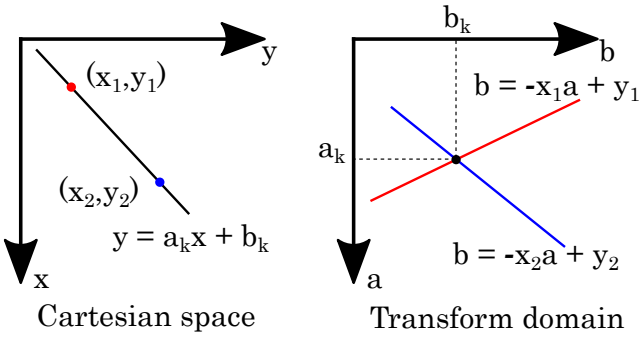

Fig. 4 The principle of the Hough transform in Cartesian coordinates with two points.

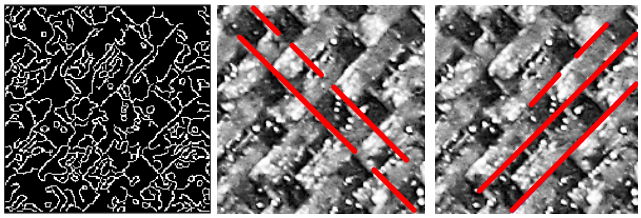

Fig. 5 Steps in the fiber angle detection using Hough transform. (a) Binary image from edge detection, (b) lines detected for Fiber 1 family (c) lines detected for Fiber 2 family.

line's perpendicular and the horizontal axis) to avoid infinite gradients of vertical lines.

The implementation of the fiber angle detection in MATLAB is now explained. The first step is to crop the image to the Region of Interest (ROI), i.e. the gage area. To ensure an even distribution of detected fiber angles throughout the ROI, the image is divided into a grid of cells, which shall be referred to as *Hough cells*. The idea is to detect a small number of lines (i.e.angles) within each Hough cell as shown in Fig. 5. The steps in the figure are elaborated in the following. First, in each Hough cell, Contrast-limited adaptive histogram equlization (CLAHE) is applied to make sure that the image utilizes the entire range of gray-scale values. Hereafter, the image is sharpened using unsharp masking. Then, the cell is ready for the edge detection using the Canny algorithm followed by the Hough transform. The Hough transform is carried out for each family of fibers where the distinction is achieved by careful choice of the θ-values to search for: Using the frame angle associated with the current image and a specified tolerance, a desired range of θ-values can be calculated. Upon completing the analysis of all Hough cells, tows in the entire sample will have been detected.

To obtain a contour plot of the shear angle distribution, a grid of so-called *Contour cells* is introduced. Notice, that these are different from the Hough cells. The following is repeated for each family of fibers. For each contour cell, the detected fiber tows enclosed by

the Contour cell are found, and the median value of the fiber angles together with the coordinates of the Contour cell center are stored in arrays. The array of Contour cell shear angles is then filtered using a 2D median filter. Next, a C^1 continuous surface is interpolated based on the coordinates and angles. Finally, the fabric shear angle distribution surface is obtained as the difference between the two interpolated surfaces.

4 Constant Shear Strain Rate Data

It is well established that prepreg fabric exhibits a rate-dependent behavior due to the presence of the viscous resin. To this end, constant shear rate data are of interest for two reasons: 1) For comparison with bias-extension test data at the same constant rate and 2) For use in forming simulation codes where test data can be input directly as the constitutive law. For instance, with the Abaqus *fabric* material model (Dassault Systèmes Simulia Corporation, 2014), stress-strain curves of constant strain rates can be input. Then by using interpolation, other strain rates are achieved in the material model. The testing at a constant shear rate is explained in the following.

4.1 Testing at a Constant Shear Rate

The approach for testing at a constant shear rate is as follows. First, a constant shear rate expression for the crosshead movement vs time is obtained. Next, this expression is approximated using linear segments such that it can be implemented in standard test machine software. In this study, the TestProfiler module in Bluehill 3 by Instron® is utilized.

For this study, the test shear rate was chosen such that it corresponds to the initial shear rate when testing at a crosshead rate of 100 mm/min. The shear rate is equal to 0.046 rad/s or 2.66 °/s.

The kinematic picture-frame relations were presented in Section 3.1. Using these equations, the following differential equation can be obtained (see also Harrison et al. (2002)):

$$\dot{\delta}(t) = \frac{L_F \dot{\gamma}}{2} \sqrt{4 - \frac{\left(\delta(t) + L_F\sqrt{2}\right)^2}{L_F^2}} \tag{4}$$

Using the initial condition $\delta(0) = 0$, a closed form solution to Eq. (4) can be obtained. The expression, $\delta(t)$, is rather long and is not presented here. It is instead visualized in Fig. 6 which consists of a crosshead movement vs. time graph and a shear-strain rate vs. time graph. The solution to Eq. (4), $\delta(t)$, (red dashed line)

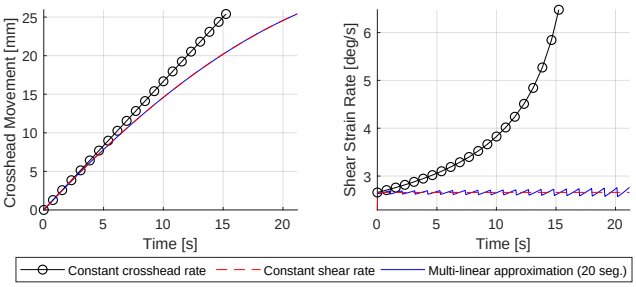

Fig. 6 Constant crosshead rate vs constant shear rate and a multi-linear approximation.

is compared to a constant crosshead rate (solid black line with circles) and the multi-linear approximation to the constant shear rate expression consisting of 20 segments (solid blue line). From Fig. 6, right graph, it is seen that the constant crosshead rate results in an increasing shear-strain rate over time. In fact, the rate increases by a factor of 2.4 over the course of the test. The constant shear-rate crosshead movement and its multi-linear approximation are indistinguishable in the graph to the left whereas differences can be observed on the graph to the right where the rate is considered. Still, the multi-linear approximation is seen to provide a good approximation of the constant shear-strain rate. The slopes of the linear segments are obtained by dividing the nonlinear expression into 20 evenly spaced time intervals and computing secants using the start and end points of each interval. All three curves displace the crosshead 25.4 mm (1 inch) which results in a frame displacement of 108 mm due to amplification linkage.

The 20 linear segments can readily be implemented as ramp segments in the TestProfiler module in Bluehill. In the first step, the crosshead is moved until the empty frame plateau load of 100 N is reached. Notice that this rather high load is an effect of the amplifying linkage mechanism. Hereafter is the actual 20 segment ramp program executed.

5 Results

This section presents the results from the sample arm geometry study using DIC and Hough transform and finally the comparison to bias-extension data.

5.1 The Influence of Sample Arm Geometry

The influence of the sample arm geometry is evaluated by two different approaches. First, the influence on the measured shear load is examined. Next, it is investigated how the different sample arm geometries affect

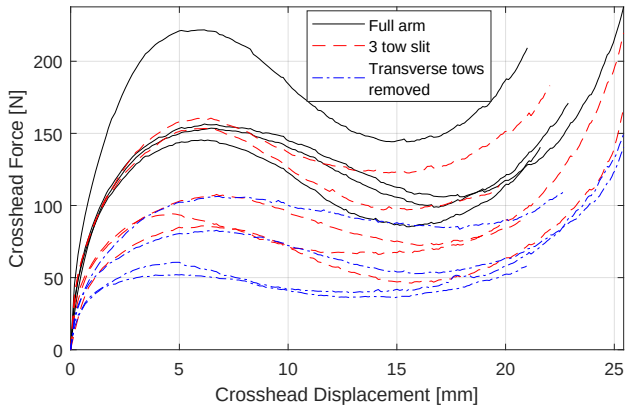

Fig. 7 Crosshead force vs. displacement curves for samples with full arms, slitted arms and arms with transverse tows removed respectively. Notice that these crosshead values are different from the frame values due to the amplifying linkage mechanism.

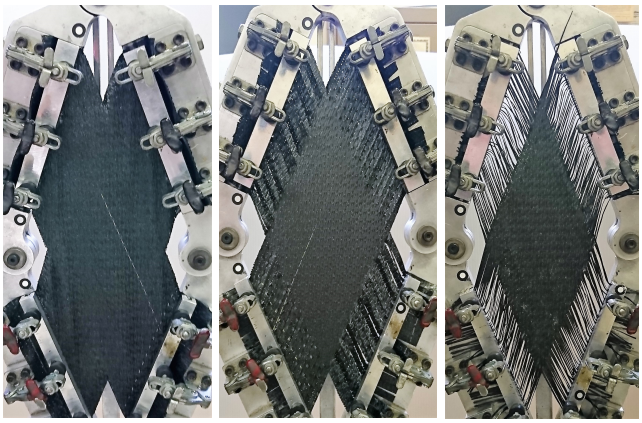

Fig. 8 Deformed samples. From left to right: Full arm, 3 tow slits and Transverse tows removed.

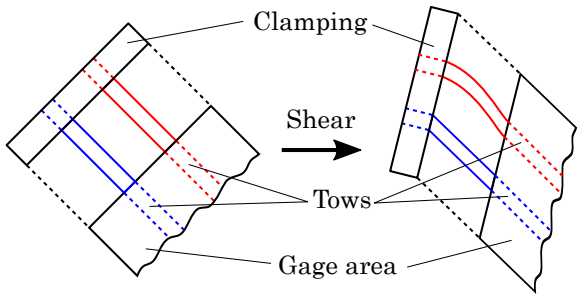

Fig. 9 Effect of in-plane tow bending stiffness on the deformation in the arm regions. Lower, blue tow has zero bending stiffness, i.e. follows kinematic assumption, whereas the upper, red tow has a finite bending stiffness.

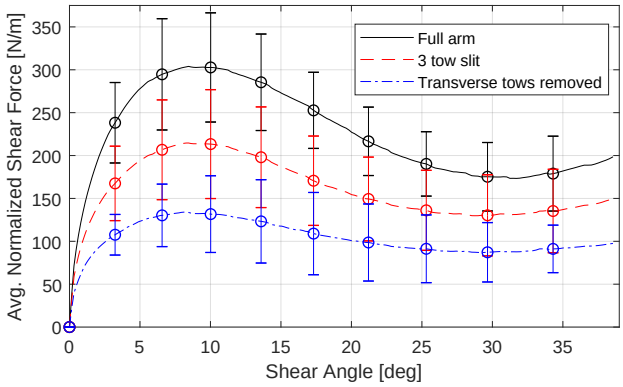

Fig. 10 Averaged values of normalized shear force vs shear angle for samples with full arms, slitted arms and arms with transverse tows removed respectively. The error bars indicate the standard deviation.

the state of the shear strain field in the gage area. Figure 7 presents the crosshead force vs crosshead displacement for all the tested samples. First of all, a lot of scatter is noticeable in the figure. As previously mentioned, the picture-frame test is sensitive to misalignments and differences in fiber tension. These sensitivities are believed to be the main causes of the scatter. Consider for instance the "Full arm" curve with the highest load in Fig. 7. During testing, this sample had very little wrinkling in the arms compared to the three other "Full arm" curves. This difference could be an indication of higher tension in the tows, but because the tow tension cannot be quantified with the setup in this study, a definitive conclusion cannot be drawn. It is worth noting that none of the "3 tow slits" or "Transverse tows removed" samples wrinkled during testing. In fact, this lack of wrinkling is a strong indication that the arm geometry does influence the samples during shearing. Fig. 8 depicts some typical deformed samples. In the figure it can be seen how the arm tows in the sample with the transverse tows removed tend to deform into S-shapes. This deformation is also sketched in Fig. 9. The boundary conditions are the same for the other sample configurations, but the resulting deformations are different. The phenomenon can be considered as instability, i.e. shear buckling of the arm regions. For the slitted samples, out-of-plane twisting of the tows between the slits can be observed. The wrinkling observed with the full-arm samples is likewise believed to arise from the clamping boundary conditions.

In general, Fig. 7 demonstrates a trend that the crosshead force decreases the more the sample arms are modified, i.e. from full arm to slitted arms and further to transverse tows removed. In Fig. 10 the crosshead data have been converted to normalized shear force vs shear angle data using Eq. (1) and (3). Each family of curves has been averaged and the standard deviation is indicated with error bars. The trend from Fig. 7 is replicated with the addition that the curves also become flatter with increasing sample arm modification.

In the following, the full-field DIC data are used to further analyze the different sample arm geometries.

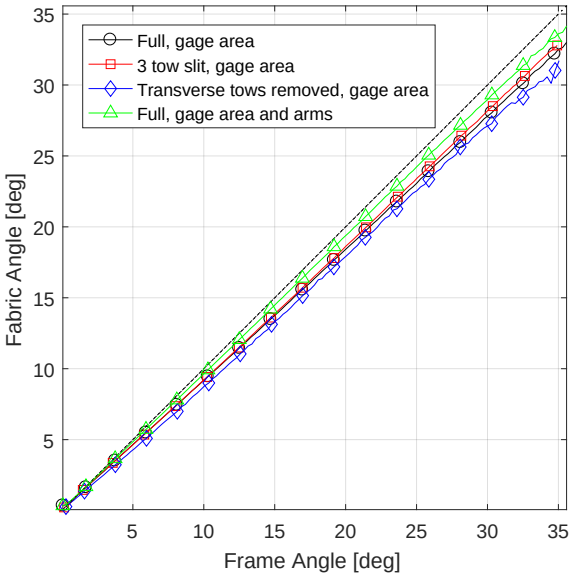

Fig. 11 DIC fabric angles vs frame angles from the gage area of full arm geometry, 3-tow slits and transverse tows removed. Also from entire sample with full arm geometry. The theoretical 1:1 line is shown as black dots.

For the samples with modified arms, no useful DIC data are available in the arms due to the discontinuity of the sample surface. These discontinuities are visible in Fig. 8.

To verify that the fabric shear angles follow the frame angles, all shear angles from each stage of the DIC data have been averaged. The averaged or *global shear angles* are plotted against the frame angle in Fig. 11. In the figure, it is seen that all of the shear angles measured in the gage area follow the frame angle well, but the difference increases with increasing frame angle. The full-arm and the 3-tow slit curves are almost indistinguishable whereas the transverse tows removed is slightly lower. It is interesting though, that the closest results are observed for the full-arm geometry with shear angles measured over the entire area of the sample.

The question is next, how the distribution of shear angles changes with the different sample-arm geometries in the study. For reference, consider the full arm geometry sample in Fig. 12. The contours covering the entire sample area indicate the distribution of the fabric shear angles at a picture-frame angle of 24°. In the gage area, the shear angles appear to be in the vicinity of 24° with some lower values near the boundaries. The arms of the sample, however, are exhibiting higher shear angles than the frame angle. This difference in the shear angles between these two regions on the test samples, explains the observations made regarding Fig. 11: The shear angles are in general up to 2° behind the frame

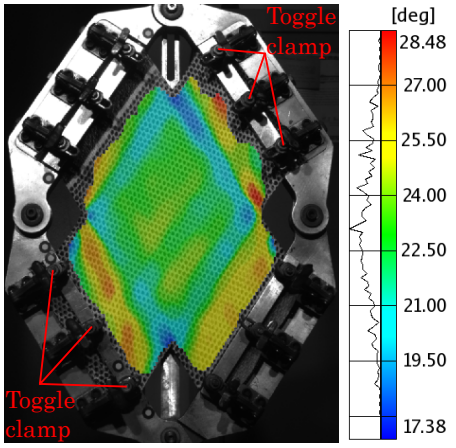

Fig. 12 Distribution of the shear angles in sample with full-arm geometry at a picture-frame angle of 24°.

angle when considering the gage area, but the higher angles observed in the arms counteract this lag when the entire sample area is used for calculating the global shear angle.

Another interesting observation can be made from Fig. 12 by looking closely at the gage area: Diagonal bands of slightly higher shear angles extend from one toggle clamp to another. These bands indicate that the clamping design does not provide a uniform amount of clamping force across the width of the sample.

Due to the aforementioned availability of the DIC data, the comparison between the shear angle distribution for the different arm geometries in Fig. 13 only concerns the gage area. In the comparison, the frame angle is 18°.

In Fig. 13, each of the contour scales has been set to the same maximum and minimum values. With aid from the histogram next to each colorbar, the following remarks can be made: The full-arm geometry and 3-tow slits samples both have a fairly uniform distribution of shear angles although the 3-tow slits sample has fewer boundary effects. In the sample with transverse tows removed, the distribution of shear angles is less uniform. The contours show the effect of uneven tension in the tows which results in shear angles that are both significantly higher and lower than the frame angle.

It must be pointed out that the DIC results only represent one sample within each configuration of arm geometry. However, because the average fabric angles follow the frame angle well, it is believed that the results from Fig. 13 are generally applicable to the the tested material system.

In general, it can be stated that the samples with transverse tows removed require a significantly lower force to be sheared compared to the full-arm samples.

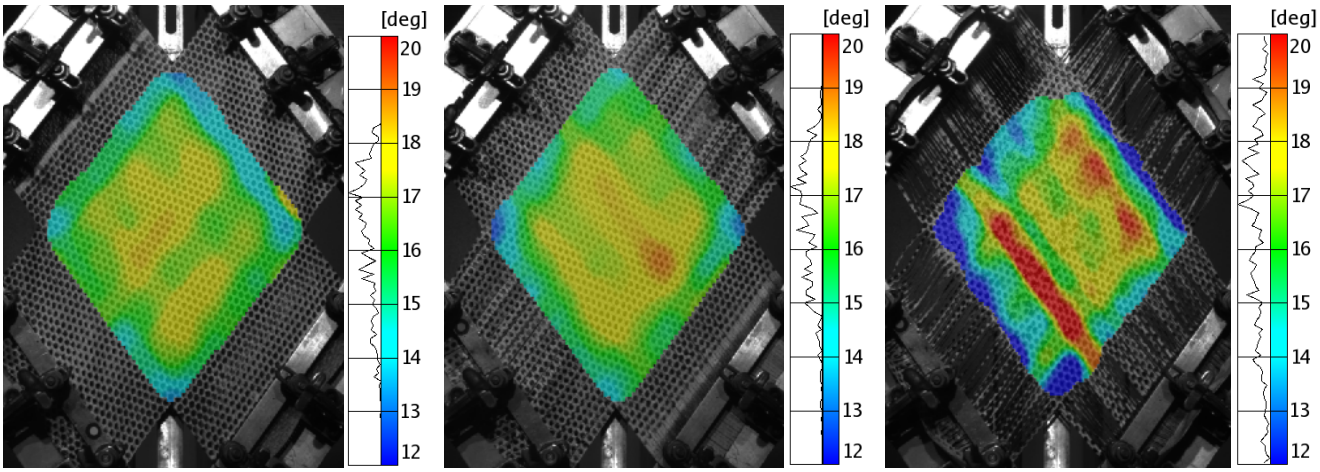

Fig. 13 Comparison of DIC shear angles in gage area for full arm geometry (left), 3 tow slits (middle) and transverse tows removed (right). The frame angle is 18°.

The DIC results indicate that the distribution of shear angles is more scattered in samples with transverse tows removed in comparison to the other sample geometries, but the average shear angle in the gage area shows only a minor lag.

5.2 Shear Angles from Hough Transform

In this paragraph, the Hough transform approach for obtaining the shear angles is evaluated. Full-field shear-angle data from 3-tow slits and transverse-tows-removed samples are presented for comparison of the Hough transform approach with the DIC results. Notice, however, that the speckle pattern on the DIC samples inhibits the detection of fiber angles from the weave texture. Further, both acquisition methods are sensitive to the right lighting conditions and thus, the same sample cannot conveniently be analyzed using both DIC and Hough transform during testing. For this reason, the Hough transform results were validated by means of manual measurements on the images acquired during the test. The Hough transform settings used are listed in Table 2.

The full-field results from the Hough transform are presented in Fig. 14 (initial configuration, i.e. undisplaced frame) and Fig. 15 (18° frame angle). It was found that the initial configuration did not have perfectly 90° tow angles as seen in Fig. 14. This pre-shear was likely induced during mounting in the frame as the figure suggests the effects of clamping. The pre-shear could also occur during preparation of the sample or even at an earlier stage. Regardless, it should receive more attention in future studies. For the purpose of comparison with the DIC results, the average shear angle from the initial configuration was subtracted from the deformed full-field data. The average initial shear angles were 1.35° (3 tow slits) and 0.46° (transverse tows removed) respectively. Pre-shear is not a new concept and was for instance investigated by Alsayednoor et al. (2017) in relation to the bias-extension test.

Table 2 Parameters used for Hough transform. Some settings are different for the fibers families due to fiber family 2 being more visible in the weave pattern. †The Hough cell vertical size is determined based on the horizontal size and the image aspect ratio. The image size is 3456 × 5184 pixels.

Parameter	Fiber 1	Fiber 2
θ tolerance rel. to frame	±10°	±10°
Number of Hough peaks	5	7
Min. length in line extraction	21 pix	25 pix
Fill gap value in line extraction	10 pix	12 pix
Hough Cell horizontal size†	165 pix	
Hough Cell overlap	50 %	
Contour Cell size	130 pix	
Contour Cell overlap	50 %	
Median filter size	5 × 5	

The Hough transform results obtained with an 18° frame angle in Fig. 15 show the same trends as observed with the DIC results in Fig. 13. The 3-tow-slits sample has a fairly uniform distribution of shear angles with some boundary effects whereas the transverse-tows-removed sample has a lot less uniform distribution. Due to noise in the results, the spatial resolution is low compared to the DIC results and a considerable amount of filtering was applied. For this reason, the present Hough transform results are only suitable for exploring the trend or for obtaining a global shear angle. Hence, by averaging the shear angles for the two contour plots in Fig. 15 respectively, global shear angles of 16.88° (3-tow slits) and 17.96° (transverse tows

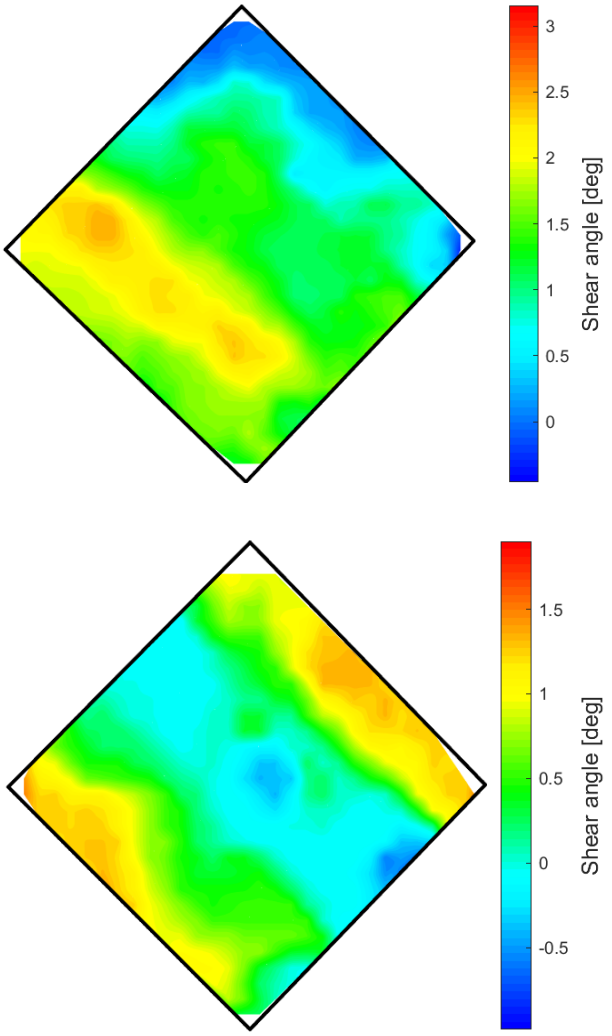

Fig. 14 Shear angles in the gage area for the undisplaced frame obtained using Hough transform. Sample configurations: 3-tow-slits (top) and transverse-tows-removed (bottom). The colorbars are centered around the mean and span ±3 standard deviations.

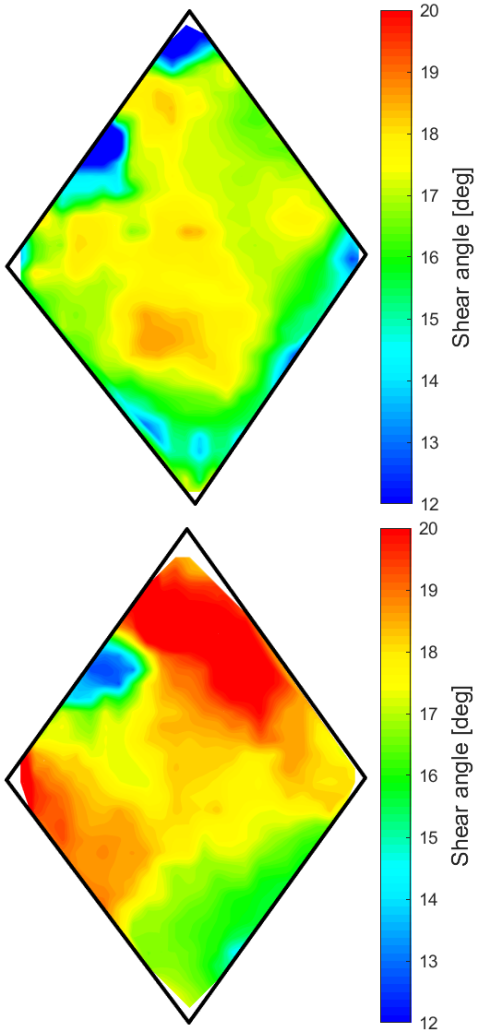

Fig. 15 Shear angles in the gage area for 18° frame angle obtained using Hough transform. Sample configurations: 3-tow-slits (top) and transverse-tows-removed (bottom).

removed) are obtained. These values compare well with the global shear angles from DIC in Fig. 11.

5.3 Comparison to Bias-Extension Data

In this section the picture-frame test results are compared to results obtained with the bias-extension test. The question is, however, what test configuration of picture-frame results should be used for the comparison. The normalized shear force curves in Fig. 10 along with the DIC results indicate that results obtained from the samples with the transverse tows removed provide the best representation of the material's shear characteristic. Recall though, that Eq. (3) from Peng et al. (2004), which was used for normalization of the picture-frame crosshead force data, assumes that only the gage area contributes to the shear force. In the same paper, the authors present a normalization equation based on the assumption that the entire sample contributes to the shear force:

$$F_{sh,norm\_entire} = \frac{L_F}{L_f^2 + 2(L_F - L_f)L_f} F_{sh} \tag{5}$$

The assumption of shear force contributions from the entire sample can be justified using Fig. 12. This figure shows, that the arms of the standard cruciform sample do indeed experience shearing to the same extent as the gage area. Thus, in the following, the picture-frame data used for comparison are the transverse-tows-removed data from Fig. 10 and the averaged full-arm crosshead data normalized with Eq. (5).

Regarding the bias-extension data, a sequence of linear ramps have been implemented in the test machine control software analogous to Sec. 4.1. Thereby

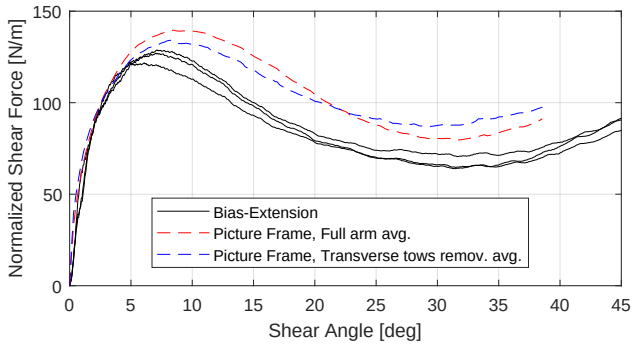

Fig. 16 Comparison between picture frame and bias-extension results.

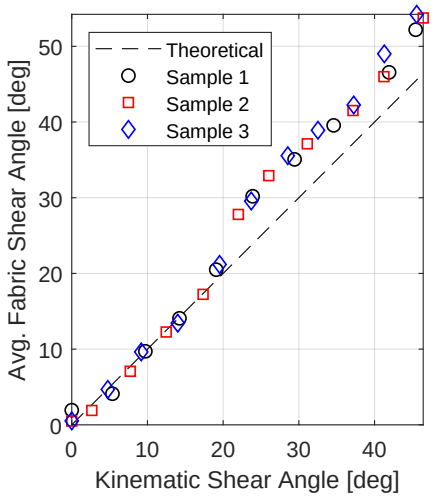

Fig. 17 Measured vs. kinematic shear angles in center region of bias-extension samples.

the same constant shear rate of 0.046 rad/s can be achieved. Three samples of 120 mm × 270 mm were tested. The load cell used had a capacity of 2 kN (0.4 % accuracy). The data processing, i.e. calculation of shear angle and normalized shear force, follows the description in Cao et al. (2008). Videos of the specimens during testing were analyzed using Hough transform to extract the average fabric shear angle in the center zone and to correct the calculated angle. The Hough transform results were again validated using manual measurements.

The comparison between picture-frame and bias-extension results is presented in Fig. 16. Regarding the bias-extension data in the figure, it is seen that the three test results are very close to each other with a maximum absolute deviation between the curves of only 10 N/m. Thus, the issue with uneven fiber tension between different samples in the picture frame test is avoided with the bias-extension test. Regarding the two sets of picture frame data, it is remarkable how the different normalization methods manage to bring the curves close to each other. Finally, comparing the picture frame data with the bias-extension data, a fairly close resemblance is observed. It must be noted that the shear force from the bias-extension test is calculated using a formula derived for dry fabrics. Thus, it naturally introduces errors.

For reference, a result from the Hough transform image analysis of the bias-extension test is presented in Fig. 17 as the average fabric shear angle vs. the kinematic shear angle. The former is the average of the measured shear angles in the center region of the specimen and the latter is obtained based on the distance between the grippers. It is seen that the measured angles follow the kinematic angles until around 20° after which they start to deviate to higher values. It is believed that this phenomenon arises from so-called 2nd gradient effects (Ferretti et al., 2014): At the boundaries between the shear zones in the sample, the in-plane bending stiffness of the tows inhibits a sharp shear angle transition. This violates the pin-jointed net assumption behind the bias-extension kinematics. The same phenomenon was e.g. also observed in the data presented in Alsayednoor et al. (2017).

6 Discussion

The work presented in this paper enables the drawing of many conclusions, but some points are up for discussion. Consider, for instance, the reason for testing the fabric at a constant shear rate and in a manner which provides a uniform shear-angle distribution in the sample: The idea is to get a more accurate shear characteristic compared to the usual test procedure. However, as was demonstrated, the modification of the sample arms resulted in more scatter in the data because the samples were more difficult to mount properly in the frame than the baseline configuration samples. The current picture-frame design with toggle clamps also caused issues in terms of the uniformity of the shear-angle field - especially with the modified samples. To this end, various design improvements of the picture frame can be found in the literature (Launay et al., 2008; Milani et al., 2010; Nosrat-Nezami et al., 2014).

Steps could of course be taken to alleviate the issues mentioned above, e.g. by keeping the fabric material intact in the part of the sample arm that is clamped. Effectively, that would mean to remove only the transverse tows in some part of the arm. However, the sample preparation used in this study was already cumbersome. Thus, the best recommendation for picture-frame testing of the prepreg fabric used in this study would be to use the original cruciform sample and normalize the

shear force assuming that the entire sample area contributes to the shear force. As was seen in Fig. 16, this approach yielded a good agreement with the modified-sample and bias-extension data.

The image processing results using the Hough transform were able to replicate the trends observed with the DIC results. A lot of noise was present in the located fiber angles which was reduced by means of filtering. One issue was glare effects due to the resin on the prepreg material. Thus, the measurement signal could maybe be improved by testing with polarized light in combination with a polarizing filter on the camera lens. Another option would be to paint a grid on the sample as utilized by Arumugam et al. (2016). Here, the grid lines should preferably be centered on the tows which could be accomplished with a stencil. However, as previously discussed, one important benefit of the present approach is that the samples are completely unaffected by the shear angle measurement.

The Hough transform method also has its limitations. In fact, it concerns a general issue for 2D measurement techniques as investigated by Alsayednoor et al. (2017): If the bias-extension sample wrinkles, the out-of-plane displacements can cause the angle-measurements to be 20% higher than the true value. In this case, a 3D technique needs to be employed. When the sample shears, the two families of tows cross over each other. Thus, the best measurements are obtained in the initial configuration. With this in mind, another possible application of the Hough transform would be only to inspect the sample in the picture frame before the start of the test. If the frame is also identified in the image, the fiber angles relative to the frame could be obtained.

Another interesting point is the influence of the modified sample arms when comparing to the similar study by Dangora et al. (2015) using pre-consolidated UD cross-ply. In that study, similar decreases in the magnitude of the crosshead force were observed with increasing arm modification but in contrast to this study, a pronounced and critical effect on the uniformness of the shear strain field in the gage area was observed. One explanation for this result is that the UD cross-ply has much less interaction between the two fiber directions which could mitigate the effects of uneven clamping forces. This underlines that one should be careful to draw general conclusions based on one material study. To this end it would be interesting to test more material systems, e.g. with different fiber architectures, different fiber materials and different matrix materials.

Conclusion

This paper has presented the results of an investigation concerning the shear characterization of woven prepreg fabric using the picture-frame test. In particular, the influence of the cruciform-sample arms, methods for acquiring shear angles and the concept of testing at constant shear-strain rates were examined.

Testing at a constant shear-strain rate was achieved by considering the kinematics of the picture frame whereby a nonlinear expression for the crosshead displacement vs. time was obtained. The nonlinear expression was implemented in the control software of the tensile-test machine by means of a series of ramp segments. Using this approach, picture-frame data can be objectively compared to bias-extension data, when the test rate is of importance.

The investigation of the influence of the sample arm geometry involved modifications to the original cruciform sample. The first modification was cutting of slits in the arms while the second was dissolving the resin and removing the transverse tows in the arms. Using DIC, it was first established that a slitted sample had a slight improvement on the uniformity of the shear-strain field compared to an original cruciform sample, whereas a sample with transverse tows removed had a less uniform distribution. The latter observation was ascribed to the fact that the sample was more difficult to mount correctly in the frame such that the tow tension was even. For all three kinds of samples the average shear angles were close to the calculated angles from the kinematics of the picture frame.

Comparing the measured crosshead forces between the three different sample geometries, a large difference was observed. Namely, the forces measured from the original sample geometries were approximately twice of those from the samples with the transverse tows removed. This difference clearly indicates that the arms of the cruciform sample influence the measured results.

Next, it was investigated if shear angles could be obtained directly from images taken during the test by using image processing. In particular, whether a Hough transform could locate the fiber directions using only the weave structure. With the setup used in this study, the approach managed to capture the trend in the shear-angle distribution when comparing to DIC and to predict the average shear angle well. There is potential for improvement, but the present results work as a proof of concept for further development.

Finally, comparing the data of the normalized shear force vs. shear angle from the picture-frame test with bias-extension test results obtained at the same constant shear-angle rate, good agreement was found. Here,

different normalization schemes for the picture-frame test shear force were employed. Namely, the original cruciform sample data were normalized assuming contributions from the gage area and the arms, whereas the transverse-tows-removed data were normalized assuming only contributions from the gage area. The two normalization schemes brought the shear force curves remarkably close to each other. Thus, the recommendation regarding picture frame testing of the prepreg material in this study, is to test the original cruciform sample and normalize assuming contributions from the entire sample.

Acknowledgments

The authors wish to thank the Innovation Fund Denmark (grant no. 5163-00003B) for providing support for the research presented in the paper. The authors also thank Terma Aerostructures A/S for providing the material.

Conflict of Interest

The authors declare that they have no conflict of interest.

References

Alsayednoor J, Harrison P, Yu WR (2017) Influence of specimen pre-shear and wrinkling on the accuracy of uniaxial bias extension test results. Composites Part A: Applied Science and Manufacturing 101:81–97, DOI 10.1016/j.compositesa.2017.06.006

Arumugam V, Mishra R, Militky J, Tunak M (2016) In-plane shear behavior of 3D spacer knitted fabrics. Journal of Industrial Textiles 46(3):868–886, DOI 10.1177/1528083715601509

Cao J, Akkerman R, Boisse P, Chen J, Cheng HS, de Graaf EF, Gorczyca JL, Harrison P, Hivet G, Launay J, Lee W, Liu L, Lomov SV, Long A, de Luycker E, Morestin F, Padvoiskis J, Peng X, Sherwood JA, Stoilova T, Tao X, Verpoest I, Willems A, Wiggers J, Yu T, Zhu B (2008) Characterization of mechanical behavior of woven fabrics: Experimental methods and benchmark results. Composites Part A: Applied Science and Manufacturing 39(6):1037–1053, DOI 10.1016/j.compositesa.2008.02.016

Dangora LM, Hansen CJ, Mitchell CJ, Sherwood JA, Parker JC (2015) Challenges associated with shear characterization of a cross-ply thermoplastic lamina using picture frame tests. Composites Part A: Applied Science and Manufacturing 78:181–190, DOI 10.1016/j.compositesa.2015.08.015

Dassault Systèmes Simulia Corporation (2014) Abaqus 6.14 Documentation: 23.4.1 Fabric material behavior

Ferretti M, Madeo A, Dell'Isola F, Boisse P (2014) Modeling the onset of shear boundary layers in fibrous composite reinforcements by second-gradient theory. Zeitschrift fur Angewandte Mathematik und Physik 65(3):587–612, DOI 10.1007/s00033-013-0347-8

Harrison P, Clifford M, Long A (2002) Constitutive modelling of impregnated continuous fibre reinforced composites micromechanical approach. Plastics, Rubber and Composites 31(2):1–12, DOI 10.1179/146580102225001409

Harrison P, Clifford M, Long A (2004) Shear characterisation of viscous woven textile composites: A comparison between picture frame and bias extension experiments. Composites Science and Technology 64(10-11):1453–1465, DOI 10.1016/j.compscitech.2003.10.015

Harrison P, Wiggers J, Long A (2008) Normalization of shear test data for rate-independent compressible fabrics. Journal of Composite Materials 42(22):2315–2344, DOI 10.1177/0021998308095367

Harrison P, Alvarez MF, Anderson D (2018) Towards comprehensive characterisation and modelling of the forming and wrinkling mechanics of engineering fabrics. International Journal of Solids and Structures 154:2–18, DOI 10.1016/j.ijsolstr.2016.11.008

Jauffrès D, Sherwood JA, Morris CD, Chen J (2010) Discrete mesoscopic modeling for the simulation of woven-fabric reinforcement forming. International Journal of Material Forming 3(SUPPL. 2):1205–1216, DOI 10.1007/s12289-009-0646-y

Krieger H, Kaufmann D, Gries T (2015) Kinematic drape algorithm and experimental approach for the design of tailored non-crimp fabrics. Key Engineering Materials 651-653:393–398, DOI 10.4028/www.scientific.net/KEM.651-653.393

Krogh C, Glud JA, Jakobsen J (2019) Modeling the robotic manipulation of woven carbon fiber prepreg plies onto double curved molds: A path-dependent problem. Journal of Composite Materials 53(15):2149–2164, DOI 10.1177/0021998318822722

Launay J, Hivet G, Duong AV, Boisse P (2008) Experimental analysis of the influence of tensions on in plane shear behaviour of woven composite reinforcements. Composites Science and Technology 68(2):506–515, DOI 10.1016/j.compscitech.2007.06.021

Lebrun G, Bureau MN, Denault J (2003) Evaluation of bias-extension and picture-frame test methods for the measurement of intraply shear properties of PP/glass commingled fabrics. Composite Structures 61(4):341–352, DOI 10.1016/S0263-8223(03)00057-6

Lomov SV, Boisse P, Deluycker E, Morestin F, Vanclooster K, Vandepitte D, Verpoest I, Willems A (2008) Full-field strain measurements in textile deformability studies. Composites Part A: Applied Science and Manufacturing 39(8):1232–1244, DOI 10.1016/j.compositesa.2007.09.014

Lussier D (2000) Shear characterization of textile composite formability. Master's thesis, University of Massachusetts, Lowell

Marques O (2011) Practical Image and Video Processing Using MATLAB. John Wiley & Sons, DOI 10.1002/9781118093467

Milani AS, Nemes JA, Lebrun G, Bureau MN (2010) A comparative analysis of a modified picture frame test for characterization of woven fabrics. Polymer Composites 31(4):561–568, DOI 10.1002/pc.20849

Mohan RP, Alshahrani H, Hojjati M (2016) Investigation of intra-ply shear behavior of out-of-autoclave carbon/epoxy prepreg. Journal of Composite Materials 50(30):4251–4268, DOI 10.1177/0021998316635238

Nguyen M, Herszberg I, Paton R (1999) The shear properties of woven carbon fabric. Composite Structures 47(1-4):767–779, DOI 10.1016/S0263-8223(00)00051-9

Nosrat-Nezami F, Gereke T, Eberdt C, Cherif C (2014) Characterisation of the shear-tension coupling of carbon-fibre fabric under controlled membrane tensions for precise simulative predictions of industrial preforming processes. Composites Part A: Applied Science and Manufacturing 67:131–139, DOI 10.1016/j.compositesa.2014.08.030

Olson BG, Krieger H, Sherwood JA, Willis DJ, Bergeron K (2017) Investigation of Tensile Properties of Braided Parachute Suspension Line. In: 24th AIAA Aerodynamic Decelerator Systems Technology Conference, American Institute of Aeronautics and Astronautics, Denver, Colorado, DOI 10.2514/6.2017-4198

Peng X, Cao J (2005) A continuum mechanics-based non-orthogonal constitutive model for woven composite fabrics. Composites Part A: Applied Science and Manufacturing 36(6):859–874, DOI 10.1016/j.compositesa.2004.08.008

Peng X, Cao J, Chen J, Xue P, Lussier DS, Liu L (2004) Experimental and numerical analysis on normalization of picture frame tests for composite materials. Composites Science and Technology 64(1):11–21, DOI 10.1016/S0266-3538(03)00202-1

Zhu B, Yu TX, Tao XM (2007) An experimental study of in-plane large shear deformation of woven fabric composite. Composites Science and Technology 67(2):252–261, DOI 10.1016/j.compscitech.2006.08.011